Multienergy gold ion implantation for enhancing the field electron emission characteristics of heterogranular structured diamond films grown on Au-coated Si substrates

K. J. Sankaran,[1,2] D. Manoharan,[3] B. Sundaravel,[4] and I. N. Lin[3,a)]
[1]*Institute for Materials Research (IMO), Hasselt University, Diepenbeek 3590, Belgium*
[2]*IMOMEC, IMEC vzw, Diepenbeek 3590, Belgium*
[3]*Department of Physics, Tamkang University, Tamsui 251, Taiwan*
[4]*Materials Science Group, Indira Gandhi Centre for Atomic Research, Kalpakkam 603 102, India*

(Received 25 July 2016; accepted 30 August 2016; published online 9 September 2016)

Multienergy Au-ion implantation enhanced the electrical conductivity of heterogranular structured diamond films grown on Au-coated Si substrates to a high level of 5076.0 $(\Omega\,\mathrm{cm})^{-1}$ and improved the field electron emission (FEE) characteristics of the films to low turn-on field of 1.6 V/μm, high current density of 5.4 mA/cm^2 (@ 2.65 V/μm), and high lifetime stability of 1825 min. The catalytic induction of nanographitic phases in the films due to Au-ion implantation and the formation of diamond-to-Si eutectic interface layer due to Au-coating on Si together encouraged the efficient conducting channels for electron transport, thereby improved the FEE characteristics of the films. *Published by AIP Publishing*. [http://dx.doi.org/10.1063/1.4962537]

Field emitters with superior field electron emission (FEE) characteristics are employed as a cold cathode materials in flat panel displays and other electron emitting devices.[1–3] Compared with the carbon-based field emitters,[4–6] diamond possesses high FEE characteristics due to its negative electron affinity (NEA),[7,8] which makes it a promising material for applications as FEE emitters. But owing to the wide bandgap nature of diamond, the electrical conductivity in bulk diamond is low, which decreases its electron emission. As a result, the high prospective that the diamond is accepted as a cold cathode field emitting material necessitates the material to be conductive. Recently, the main focus has been directed towards the synthesis of the ultrananocrystalline diamond (UNCD) film, containing the ultra-small diamond grains of 5–10 nm with smooth surface characteristics, which exhibits higher electrical conductivity and better FEE properties than the other form of diamond films.[9,10] The sp^2-bonded carbon in the grain boundaries of UNCD films is conceived as the electron conduction channel in FEE.[11–14] However, the electrical conductivity of non-diamond carbon contained in the grain boundaries of UNCD films is not sufficiently high and therefore limits the FEE properties of UNCD films. Thus, the diamond films of high sp^3-bonded carbon content with grain boundaries phase of better conductivity are desperately needed for the development of better FEE materials.

In this letter, multienergy Au ions were implanted on heterogranular structured diamond (HGD) films grown on the Au-coated Si substrates for improving their electrical conductivity and the FEE characteristics. The detailed microstructures of the multienergy Au-ion implanted HGD films were investigated using transmission electron microscopy (TEM) and the role of Au in enhancing the FEE characteristics of these HGD films was discussed.

100 nm Au deposited Si (Au(Si)) substrates were used to grow diamond films. Prior to Au deposition, a thin layer of Cr (~5 nm) was deposited on Si to achieve strong adhesion of Au on Si. The process of Au and Cr deposition on Si and the pre-seeding process for the growth of diamond on these Au(Si) substrates are described in detail elsewhere.[15,16] The UNCD films were first deposited using microwave plasma enhanced chemical vapor deposition (MPECVD) system in Ar(99%)/CH_4(1%) plasma under 1200 W and 120 Torr for 90 min. The plane view scanning electron microscopy (SEM; Jeol 6500) image shown in Fig. S1 of the supplementary material depicts that the UNCD films have a very smooth surface. The high resolution transmission electron microscopy (HRTEM; Jeol 2100F) investigation (Fig. S2, supplementary material) indicated that these films contain spherical ultra-small diamond grains (~5 nm) with grain boundaries of considerable thickness (~0.2 nm). Subsequently, a secondary MPECVD process using a Ar(49%)/H_2(50%)/CH_4(1%) gas with 55 Torr chamber pressure and 1500 W microwave power was performed for 120 min.[17] These films were designated as HGD/Au(Si) films. The surface morphology of the HGD/Au(Si) films appears faceted morphology with large diamond grains of micron size (inset "I" of Fig. 1(a)).

Au ions are then implanted in the HGD/Au(Si) films at various energies from 400 keV to 3850 keV corresponding to ion ranges from 98 nm to 700 nm with different fluences, which is shown in Fig. 1(a), totaling to a fluence of 1×10^{16} ions/cm^2 and the obtained films were designated as Au-HGD/Au(Si) films. The multienergy Au-ion implantation process rendered the surface morphology of the Au-HGD/Au(Si) films to equiaxed nanosized diamond grains of size around 20–30 nm (inset "II" of Fig. 1(a)) that is contrary to the case when the UNCD films were implanted by single energy 500 keV Au-ions with the fluence of 1×10^{17} ions/cm^2 (single Au-UNCD) that resulted in a featureless surface morphology for the the UNCD films.[18] The energy dispersive X-ray spectroscopy (EDX) spectrum (Fig. S3, supplementary material) corresponding to

a)Electronic mail: inanlin@mail.tku.edu.tw

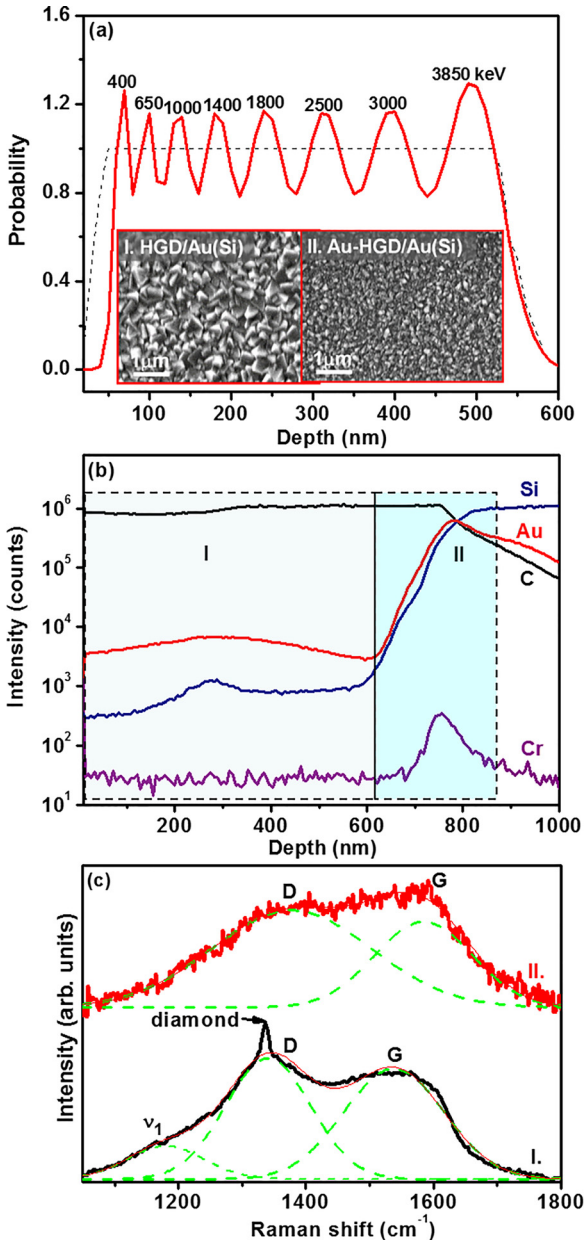

FIG. 1. (a) Multienergy implantation scheme showing the Au concentration profile simulated using the SRIM program with SEM images of (I) HGD/Au(Si) and (II) Au-HGD/Au(Si) films shown as insets; (b) SIMS depth profiles of C, Au, Cu, and Si species in the Au-HGD/Au(Si) films; (c) visible-Raman spectra of (I) HGD/Au(Si) and (II) Au-HGD/Au(Si) films.

the SEM image of the Au-HGD/Au(Si) films (inset "II" of Fig. 1(a)) clearly shows the Si and Au peaks indicating the existence of Si and Au species in the Au-HGD/Au(Si) films. To facilitate the comparison, the HGD films were also grown directly on Si, followed by the multienergy Au-ion implantation process and thus obtained films were designated as Au-HGD/Si.

The secondary ion mass spectroscopy (SIMS; Cameca IMS-4f) depth profile shown in Fig. 1(b) suggests that the Au ions are distributed uniformly throughout the thickness of the implanted region (region "I" of Fig. 1(b)) of the Au-HGD/Au(Si) films. This is contrary to the SIMS results of single Au-UNCD films, in which the Au ions are non-uniformly distributed to a depth of about 320 nm with peak concentration located at around 160 nm beneath the surface.[18] Region "II" of Fig. 1(b) clearly shows that there are pronounced Au- and Si-ion counts observed in the interface layer, inferring the marked diffusion of Au and Si species into the interface layer. The Au(Si) counts drop rapidly away from the interface to the surface of diamond films. In addition, the Cr ions were also observed near to the interface of diamond and Si (region "II" of Fig. 1(b)), implying that the presence of Cr has evidently enhanced the adhesion of Au-layer.

Fig. 1(c) shows the visible-Raman spectra ($\lambda = 632.0$ nm, spectral resolution 0.5 cm^{-1}, Lab Raman HR800, Jobin Yvon) of the I. HGD/Au(Si) and II. Au-HGD/Au(Si) films, which were deconvoluted using the multi-peak Lorentzian fitting method. Spectrum I in this figure shows that the Raman spectrum of the HGD/Au(Si) films contains a sharp peak at 1336 cm^{-1} corresponding to sp^3-bonded carbon (diamond) and the broadened peaks at around 1375 cm^{-1} (D-band) and 1536 cm^{-1} (G-band) corresponding to the disordered and graphitic phase, respectively.[19–21] There also exists a peak at around 1169 cm^{-1}, which is attributed to the ν_1 mode of *trans*-polyacetylene present in the grain boundaries.[22] The existence of diamond peak at 1336 cm^{-1} is related to the formation of large diamond grains due to the coalescence process that resulted in the faceted micron-sized diamond grains in the HGD/Au(Si) films (cf. inset "I" of Fig. 1(a)). It is to be noted that in the UNCD films (primary layered diamond films), all the Raman peaks are very broad (Fig. S4, supplementary material) that is ascribed to the ultra-nano sized diamond grains in the UNCD films. Spectrum II of Fig. 1(c) shows the effect of multienergy Au-ion implantation on altering the bonding characteristics of the Au-HGD/Au(Si) films. It shows higher intensity D and G peaks with noisy background, implying the amorphization or graphitization type of transitions with some blue shifting of the G band. The Raman spectra show the I_D/I_G values (ratio of intensities of D-peak to G-peak) of 0.85 and 1.10 for HGD/Au(Si) and Au-HGD/Au(Si) films, respectively. The increase in the I_D/I_G value from 0.85 to 1.10 implies the formation of nanographitic phase and decreases in the sp^3 content from amorphous carbon (*a-C*) phase.[22] The phenomenon that the peak related to diamond is not visible in the Au-HGD/Au(Si) films can be attributed to the two possible interaction induced by the multienergy Au-ion implantation process: (1) the large grains in the Au-HGD/Au(Si) films have been converted into nano-sized diamond grains and (2) the induction of large proportion of sp^2-bonded carbon to which visible-Raman spectroscopy is more sensitive, as compared to those of sp^3-bonded carbons.[21] More detailed investigation on the microstructure/bonding structure of these films will be discussed later using electron energy loss spectroscopy (EELS; Gatan Enfina) in a transmission electron microscopy (TEM).

Hall measurements carried out in a van der Pauw configuration revealed that the multienergy Au-ion implantation markedly improved the electrical conductivity of the films. The Au-HGD/Au(Si) films exhibit high electrical conductivity of $\sigma_{\text{Au-HGD/Au(Si)}} = 5076.0\ (\Omega\ \text{cm})^{-1}$ with the sheet carrier concentration of $n_e = 9.9 \times 10^{18}\ \text{cm}^{-2}$ and mobility of $\mu_e = 130.0\ \text{cm}^2/\text{V s}$, which are superior than those of other conducting diamond films reported in literature (see Table I).[18,23–28] In contrast, the HGD/Au(Si) films

TABLE I. Comparison between the electrical conductivity and the field electron emission characteristics of the Au-HGD/Au(Si) films and other conducting diamond films.

Materials	Electrical conductivity $(\Omega\,\mathrm{cm})^{-1}$	Turn-on field (V/μm)	FEE current density (mA/cm^2)
Au-ion implanted UNCD/Si[18]	185.0	4.7	4.5 @ 8.1 V/μm
N-ion implanted UNCD/Si[23]	…	8.8	5.4 @ 20.0 V/μm
O-ion implanted UNCD/Si[24]	33.3	…	…
P-ion implanted UNCD/Si[25]	0.09	…	…
Cu-ion implanted UNCD/Si[26]	95.0	4.8	3.6 @ 8.0 V/μm
Pt-ion implanted UNCD/Si[27]	94.0	4.17	5.1 @ 7.2 V/μm
Nitrogen doped diamond nanowires[28]	186.0	4.35	3.4 @ 9.1 V/μm
Au-HGD/Au(Si) (this study)	5076.0	1.60	5.4 @ 2.6 V/μm

possess lower σ–value of 207.2 $(\Omega\,\mathrm{cm})^{-1}$ ($n_e = 3.6 \times 10^{17}\,\mathrm{cm}^{-2}$ and $\mu_e = 0.85\,\mathrm{cm}^2/\mathrm{V\ s}$), whereas the Au-HGD/Si films possess the σ–value lower than that of the Au-HGD/Au(Si) films, i.e., $\sigma_{\text{Au-HGD/(Si)}} = 828.4\ (\Omega\,\mathrm{cm})^{-1}$ ($n_e = 3.2 \times 10^{18}\,\mathrm{cm}^{-2}$ and $\mu_e = 75.8\,\mathrm{cm}^2/\mathrm{V\ s}$). Apparently, the multienergy Au-ion implantation process is the main factor, which converts the HGD films into highly conducting diamond films. The presence of the Au-interlayer less markedly altered the Hall conductivity of the HGD films, as this Hall technique measures the conductivity along the surface rather than crossing the interface.

The FEE behaviors of these highly conducting Au-HGD/Au(Si) films are shown in Fig. 2, which reveal the fascinating FEE properties of these films. The details of the FEE experiments are given elsewhere[15] and the FEE properties of these films were analyzed using the Fowler Nordheim (FN) theory.[29] The plots of $\ln(J/E^2)$–$1/E$ (curve I, Fig. 2(b)) show that the E_0 value of 1.60 V/μm was attained for Au-HGD/Au(Si), which is lower than those of the E_0 values of HGD/Au(Si) ($(E_0)_{\text{HGD/Au(Si)}} = 4.23$ V/μm; curve II, Fig. 2(b)) and Au-HGD/Si films ($(E_0)_{\text{Au-HGD/Si}} = 4.47$ V/μm; curve III, Fig. 2(b)). To reach a large J-value of 3.0 mA/cm^2, it needs an applied field of $E = 2.48$ V/μm for the Au-HGD/Au(Si) films (curve I, Fig. 2(a)), which is smaller than those for HGD/Au(Si) ($(E)_{\text{HGD/Au(Si)}} = 7.50$ V/μm; curve II, Fig. 2(a)) and Au-HGD/Si films ($(E)_{\text{Au-HGD/Si}} = 6.56$ V/μm; curve III, Fig. 2(b)). The effective work functions of these diamond films calculated from the slope of the FN plots (Fig. 2(a)) are $(\varphi_{\text{eff}})_{\text{Au-HGD/Au(Si)}} = 0.0127$ eV for Au-the HGD/Au(Si) films and $(\varphi_{\text{eff}})_{\text{HGD/Au(Si)}} = 0.0250$ and $(\varphi_{\text{eff}})_{\text{Au-HGD/Si}} = 0.0197$ eV for the HGD/Au(Si) and Au-HGD/Si films, respectively, revealing a low work function value for the Au-HGD/Au(Si) films. In addition, the Au-HGD/Au(Si) films shows a good lifetime stability. The FEE J versus time curve is displayed in the inset of Fig. 2(a), signifying the emission current variations recorded over a period of 1825 min at a working field of 2.4 V/μm, corresponding to a J of 1.5 mA/cm^2, for the Au-HGD/Au(Si) films. Consequently, the Au-HGD/Au(Si) films exhibit a far more efficient FEE behavior, viz., lower E_0, higher J and longer lifetime as compared with the other conducting diamond based field emitters, which are summarized in Table I.[18,23–28]

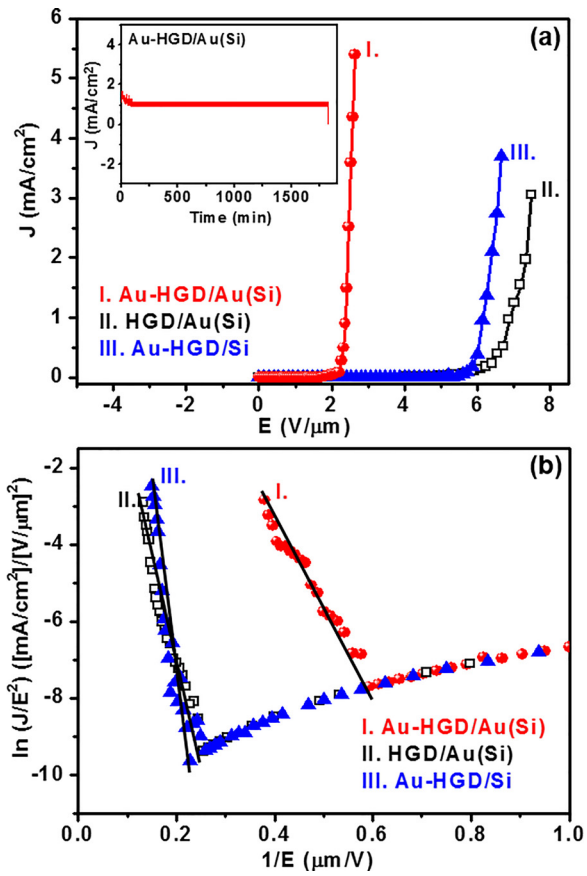

FIG. 2. (a) Field electron emission characteristics (current density-applied field, J-E, curves) measured in high vacuum environment for (I) Au-HGD/Au(Si), (II) HGD/Au(Si), and (III) Au-HGD/Si films. (b) The Fowler Nordheim (FN) plots corresponding to the J-E curves in "a". The inset of "a" shows the lifetime stability measurements (J-time curves) for the Au-HGD/Au(Si) films.

The TEM examination has been carried out to elucidate the source of enhancement on the electrical conductivity and the FEE behavior of the Au-HGD/Au(Si) films. Fig. 3(a) shows the typical bright field (BF) TEM micrograph for the Au-HGD/Au(Si) films. The corresponding selective area diffraction (SAED) pattern (inset, Fig. 3(a)) contains sharp diffraction rings corresponding to the (111), (220), and (311) diamond lattices, which confirm that the nanosized clusters are of diamond structure. A diffused ring appears in the center of the SAED pattern, indicating the existence of the sp^2-bonded carbon (graphitic or *a-C* phase). Dark-field images were taken from different parts of SAED, i.e., from the diffraction spots corresponding to diamond and graphite separately and the images were then superimposed to clearly illustrate the distribution of these phase constituents. Figure 3(b) clearly shows that the graphitic phases (green color) were uniformly distributed among

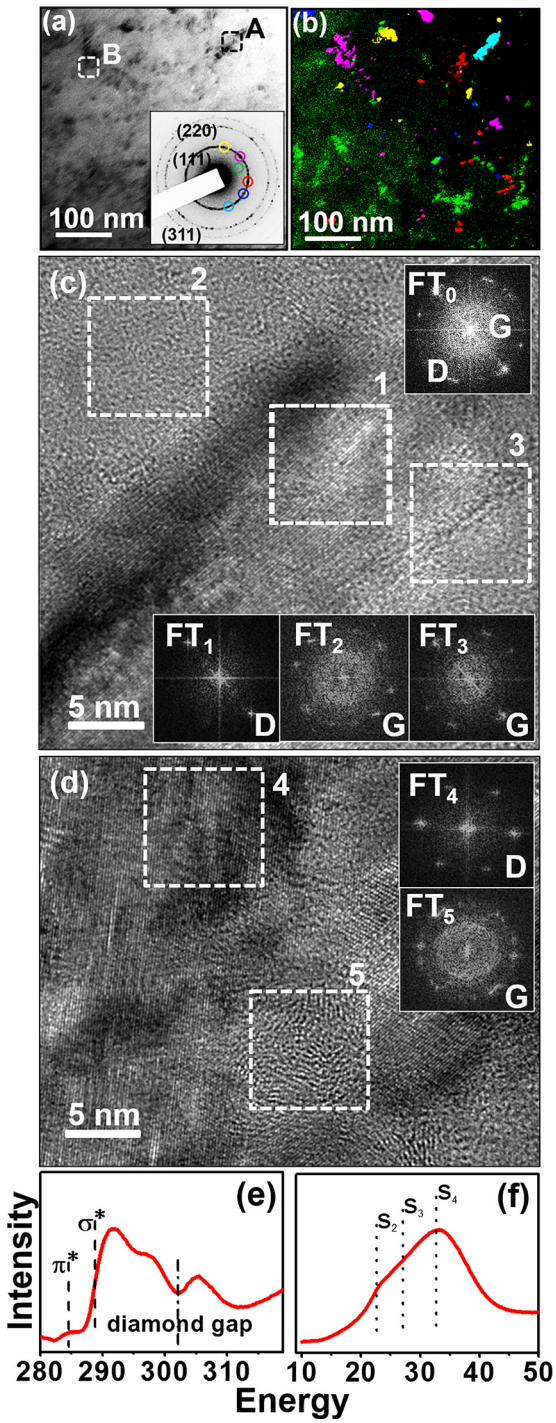

FIG. 3. The (a) bright-field with corresponding SAED pattern shown as inset and (b) dark field TEM micrographs of the Au-HGD/Au(Si) films; (c) and (d) HRTEM images of Au-HGD/Au(Si) films, corresponding to the regions "A" and "B" of "a," respectively. The inset FT_0 of "a" shows the Fourier-transformed images corresponding to the whole structure image. The FT_1–FT_5 images show the FT images corresponding to regions "1–5" of "c" and "d," respectively; (e) carbon edge core-loss EELS spectrum and (f) plasmon-loss EELS spectrum of the Au-HGD/Au(Si) films.

the diamond grains (pink, blue, and yellow colors) in the Au-HGD/Au(Si) films.

More detailed microstructure of the Au-HGD/Au(Si) films was exemplified by HRTEM studies. Fig. 3(c) shows the structure image corresponding to region "A" in the BF-TEM image of Fig. 3(a). Fourier transformed (FT) diffractogram image of the entire structure image (FT_0) in Fig. 3(c) shows a spotted diffraction pattern arranged in ring, suggesting the nano-sized nature of the diamond (D) phases. The donut-shaped diffused diffraction ring located at the center of FT_0 image indicated that the sp^2-bonded carbon corresponds to graphitic (G) phase rather than *a-C* phase. The existences of the diamond (D) phase is highlighted by region "1" and that of the graphitic phases by regions "2" and "3" and are identified by the FT images FT_1–FT_3, respectively. Sometime, the whole nano-sized diamond grains were converted into nanographite clusters, which is illustrated as curved fringes in region "5" of Fig. 3(d), which is the structure image corresponding to region "B" of the BF-TEM image (Fig. 3(a)). The corresponding FT_5-image shows a central diffuse ring of donut geometry, clearly indicates that the curved fringes in region "5" are the nanographite clusters about 5 nm in size, which is the same size of a diamond grains in small-grain regions of the HGD films.[17]

Figure 3(e) shows the selective area core-loss EELS spectrum of the Au-HGD/Au(Si) films signifying a small hump, denoting sp^2-bonded carbon (~285 eV, π^*-band), besides the typical EELS signal of the sp^3-bonded carbon, which includes a sharp peak at ~292 eV (σ^*-band) and a dip in the vicinity of ~302 eV.[30–32] Fig. 3(f) shows the selective area plasmon-loss EELS spectrum of the same region as that for core-loss EELS spectrum of the Au-HGD/Au(Si) films. The detailed deconvolution of this spectrum indicated that the Au-HGD/Au(Si) films are dominated by S_2 (~23 eV) and S_4 (~33 eV) bands along with the S_3-band (~27 eV),[31] representing that the region comprises some graphitic phases with no 22 eV peak corresponding to *a-C* phase besides the diamond phases. On the basis of TEM and EELS investigations for the Au-HGD/Au(Si) films, it is noticed that the multienergy Au-ion implantation process primarily induces the formation of nanographitic phases.

To be as a very good electron field emitter, the critical point is the supply of adequate electrons from the substrates (the Si) to the emitting sites (the diamond), besides the low work function of the emitting surface. Both the electrical conductivity of the diamond and the resistance of diamond-to-Si interface need to be optimized for improving the effectiveness for the supply of electrons. These two critical requirements are concurrently satisfied by the incorporation of Au species in the diamond films that were either precoated on the Si substrates prior to the growth of diamond films or were implanted into the diamond films. This is illustrated in region II of SIMS (cf. Fig. 1(b)) that there is a formation of Au(Si) eutectic layer in the interface between diamond and Si due to the utilization of Au coating. Hence, the formation of Au(Si) eutectic layer eliminates the origin of the *a-C* phase in the vicinity of interface, which lowers the resistivity of the interface layer.[15,16] Seemingly, the SiC was formed due to the interaction of Si and C species, i.e., the Si species have diffused through the Au(Si) eutectic layer to react with the carbon promptly, forming SiC. The SiC can enhance the efficiency for the nucleation of diamond.[16] On the other hand, region I of the SIMS studies (cf. Fig. 1(b)) revealed that the multienergy Au-ions implanted into the HGD films were uniformly distributed throughout the thickness of the films. The presence of Au in the HGD films can catalytically induce the formation of the grain boundary phase and even

converts the whole nano-sized diamond grains into the nanographitic clusters that improve the electrical conductivity of the films.[33,34] Restated, both the conductivity of diamond-to-Si interface and the bulk diamond films were enhanced due to the Au-coating and Au-ion implantation, respectively. Therefore, the electrons can be transferred effortlessly from the Si substrate across the interfacial layer to the diamond region and can move through the conduction channels of the diamond grains to the emitting surface and are then emitted to vacuum easily as the diamond surfaces are NEA in nature.[7,8]

In summary, a feasible way of fabricating highly conducting Au-HGD/Au(Si) films with enhanced FEE properties, due to multienergy Au-ion implantation process and the use of Au(Si) eutectic layer, is demonstrated. The catalytic induction of the nanographitic phases in the grain boundaries due to the Au-ion implantation advances the conducting nature of the films. Besides, the formation of the Au(Si) eutectic layer due to Au-coating induces the formation of SiC phases in the interface that efficiently nucleating the diamond, eliminating the formation of *a-C* phase, and improves the transport of electrons crossing the diamond-to-Si interface. Consequently, the superior FEE characteristics of conducting Au-HGD/Au(Si) films are achieved which may open up a pathway for the application in high-definition flat panel displays or plasma devices.

See supplementary material for SEM, Raman, and HRTEM studies of the UNCD films and the EDX spectrum of the Au-HGD/Au(Si) films.

The authors would like to thank the financial support of Ministry of Science and Technology, Taiwan through the Project Nos. MOST 104-2112-M-032-003. K. J. Sankaran is a Postdoctoral Research Fellow of the Research Foundations-Flanders (FWO).

[1]W. Zhu, G. P. Kochanski, and S. Jin, Science **282**, 1471 (1998).
[2]K. Okano, K. Hoshina, M. Iida, S. Koizumi, and T. Inuzuka, Appl. Phys. Lett. **64**, 2742 (1994).
[3]W. L. Wang, J. D. Fabbri, T. M. Willey, J. R. I. Lee, J. E. Dahl, R. M. K. Carlson, P. R. Schreiner, A. A. Fokin, B. A. Tkachenko, N. A. Fokina, W. Meevasana, N. Mannella, K. Tanaka, X. J. Zhou, T. van Buuren, M. A. Kelly, Z. Hussain, N. A. Melosh, and Z.-X. Shen, Science **316**, 1460 (2007).
[4]A. M. Rao, D. Jacques, R. C. Haddon, W. Zhu, C. Bower, and S. Jin, Appl. Phys. Lett. **76**, 3813 (2000).
[5]H. Kiyota, H. Araki, H. Kobayashi, T. Shiga, K. Kitaguchi, M. Iida, H. Wang, T. Miyo, T. Kurosu, K. Inoue, I. Saito, M. Nishitani Gamo, I. Sakaguhi, and T. Ando, Appl. Phys. Lett. **75**, 2331 (1999).
[6]B. S. Satyanarayana, A. Hart, W. I. Milne, and J. Robertson, Appl. Phys. Lett. **71**, 1430 (1997).
[7]M. W. Geis, N. N. Efremow, K. E. Krohn, J. C. Twichell, T. M. Lyszczarz, R. Kalish, J. A. Greer, and M. D. Tabat, Nature **393**, 431 (1998).
[8]H. Yamaguchi, T. Masuzawa, S. Nozue, Y. Kudo, I. Saito, J. Koe, M. Kudo, T. Yamada, Y. Takakuwa, and K. Okano, Phys. Rev. B **80**, 165321 (2009).
[9]A. R. Krauss, O. Auciello, M. Q. Ding, D. M. Gruen, Y. Huang, V. V. Zhirnov, E. I. Givargizov, A. Breskin, R. Chechen, E. Shefer, V. Konov, S. Pimenov, A. Karabutov, A. Rakhimov, and N. Suetin, J. Appl. Phys. **89**, 2958 (2001).
[10]D. Zhou, D. M. Gruen, L. C. Qin, T. G. McCauley, and A. R. Krauss, J. Appl. Phys. **84**(4), 1981 (1998).
[11]E. J. Correa, Y. Wu, J. G. Wen, R. Chandrasekharan, and M. A. Shannon, J. Appl. Phys. **102**, 113706 (2007).
[12]X. Lu, Q. Yang, C. Xiao, and A. Hirose, Thin Solid Films **516**, 4217 (2008).
[13]K. J. Sankaran, K. Srinivasu, H. C. Chen, C. L. Dong, K. C. Leou, C. Y. Lee, N. H. Tai, and I. N. Lin, J. Appl. Phys. **114**, 054304 (2013).
[14]H. C. Chen, U. Palnitkar, W. F. Pong, I. N. Lin, A. P. Singh, and R. Kumar, J. Appl. Phys. **105**, 083707 (2009).
[15]K. J. Sankaran, K. Panda, B. Sundaravel, H. C. Chen, I. N. Lin, C. Y. Lee, and N. H. Tai, ACS Appl. Mater. Interfaces **4**, 4169 (2012).
[16]H. C. Chen, K. J. Sankaran, S. C. Lo, L. J. Lin, N. H. Tai, C. Y. Lee, and I. N. Lin, J. Appl. Phys. **112**, 103711 (2012).
[17]C. S. Wang, H. C. Chen, H. F. Cheng, and I. N. Lin, J. Appl. Phys. **107**, 034304 (2010).
[18]K. J. Sankaran, H. C. Chen, C. Y. Lee, N. H. Tai, and I. N. Lin, Appl. Phys. Lett. **102**, 061604 (2013).
[19]A. C. Ferrari and J. Robertson, Phys. Rev. B: Condens. Matter Mater. Phys. **63**, 121405 (2001).
[20]J. Michler, Y. Von Kaenel, J. Stiegler, and E. Blank, J. Appl. Phys. **83**(1), 187 (1998).
[21]A. C. Ferrari and J. Robertson, Phys. Rev. B: Condens. Matter Mater. Phys. **61**, 14095 (2000).
[22]Z. Sun, J. R. Shi, B. K. Tay, and S. P. Lau, Diamond Relat. Mater. **9**, 1979 (2000).
[23]R. Arenal, P. Bruno, D. J. Miller, M. Bleuel, J. Lal, and D. M. Gruen, Phys. Rev. B **75**, 195431 (2007).
[24]X. J. Hu, J. S. Ye, H. J. Liu, Y. G. Shen, X. H. Chen, and H. Hu, J. Appl. Phys. **109**, 053524 (2011).
[25]X. J. Hu, J. S. Ye, H. Hu, X. H. Chen, and Y. G. Shen, Appl. Phys. Lett. **99**, 131902 (2011).
[26]K. J. Sankaran, K. Panda, B. Sundaravel, N. H. Tai, and I. N. Lin, J. Appl. Phys. **115**, 063701 (2014).
[27]K. J. Sankaran, K. Panda, B. Sundaravel, N. H. Tai, and I. N. Lin, J. Mater. Chem. C **3**, 2632 (2015).
[28]K. J. Sankaran, Y. F. Lin, W. B. Jian, H. C. Chen, K. Panda, B. Sundaravel, C. L. Dong, N. H. Tai, and I. N. Lin, ACS Appl. Mater. Interfaces **5**, 1294 (2013).
[29]R. H. Fowler and L. Nordheim, Proc. R. Soc. London, Ser. A **119**, 173 (1928).
[30]D. M. Gruen, S. Liu, A. R. Krauss, J. Luo, and X. Pan, Appl. Phys. Lett. **64**(12), 1502 (1994).
[31]P. Kovarik, E. B. D. Bourdon, and R. H. Prince, Phys. Rev. B **48**, 12123 (1993).
[32]I. Jimenez, M. M. Garcia, J. M. Albella, and L. J. Terminello, Appl. Phys. Lett. **73**, 2911 (1998).
[33]A. Oya and S. Otani, Carbon **17**, 131 (1979).
[34]W. Lu, K. Komvopoulos, and S. W. Yeh, J. Appl. Phys. **89**, 2422 (2001).